American Mineralogist, Volume 90, pages 247–251, 2005

Variable-temperature structural studies of tetranatrolite from Mt. Saint-Hilaire: Synchrotron X-ray powder diffraction and Rietveld analysis

YONGJAE LEE,[1,2,*] JOSEPH A. HRILJAC,[3] AND THOMAS VOGT[1,2]

[1]Physics Department, Brookhaven National Laboratory, Upton, New York 11973, U.S.A.
[2]Center for Functional Nanomaterials, Brookhaven National Laboratory, Upton, New York 11973-5000, U.S.A.
[3]School of Chemistry, University of Birmingham, Birmingham B15 2TT, U.K.

ABSTRACT

The temperature-dependent evolution of the crystal structure of natural tetranatrolite (Mt. Saint-Hilaire, approximate formula $Na_{5.85}Ca_{1.90}Al_{9.25}Si_{10.75}O_{40}\cdot 11H_2O$) was investigated using monochromatic synchrotron X-ray powder diffraction and Rietveld analysis. The room-temperature structural model reveals characteristic Al/Si and Na/Ca disordering over the framework tetrahedral and nonframework cation sites, respectively. Water molecules at the OW4 and OW5 sites along the elliptical channels surround the nonframework cations with full and partial occupancies, respectively, similar to what was observed in previous single crystal studies. As the temperature increases up to 300 °C, the partially occupied OW5 site is gradually dehydrated whereas the fully occupied OW4 site and the disordered Na/Ca site remain fully occupied. Upon complete dehydration of the OW5 site at 300 °C, another phase appears with ~1.8% expansion and ~6.7% reduction of the *a*- and *c*-axis parameters, respectively, leading to an overall volume reduction of ~3.3%. In this new phase, the Na and Ca atoms migrate to occupy two closely separated sites along the channels, and 80% of the OW4 water is lost with the remaining water molecules occupying a site close to the previously empty OW5 site. The material decomposes upon full dehydration near 400 °C and becomes X-ray amorphous. The temperature-dependent variations of the T-O-T angles and the chain rotation angle are indicative of the framework relaxation occurring during the selective dehydration and subsequent cation-water migration phase transition.

INTRODUCTION

Zeolites are naturally occurring aluminosilicates which adopt a variety of low-density framework structures constructed from corner-connected (Al,SiO_4)-tetrahedra (Breck 1984). The framework contains windows which connect to pores and channels of molecular dimensions where charge-balancing cations are located and water molecules can be absorbed. The structure of natrolite, $Na_{16}Al_{16}Si_{24}O_{80}\cdot 16H_2O$, was first proposed by Pauling and Taylor in the early 1930s (Pauling 1930; Taylor et al. 1933). Its framework is composed of so-called fibrous chains of tetrahedra interconnected to form elliptical channels along the *c*-axis (Baur et al. 1990; Meier 1960). In the parent phase, silicon and aluminum atoms are ordered at the framework tetrahedral (T) sites, and sodium cations and water molecules also adopt ordered arrangements along the channel. Chemical substitutions can occur both in the natrolite framework and charge-balancing cation sites, giving rise to a variety of analog mineral species such as scolecite, $Ca_8Al_{16}Si_{24}O_{80}\cdot 24H_2O$ (Kvick et al. 1985), mesolite, $Na_{5.3}Ca_{5.3}Al_{16}Si_{24}O_{80}\cdot 21.3H_2O$ (Artioli et al. 1986), gonnardite (Artioli and Galli 1999), and tetranatrolite (Evans et al. 2000). In scolecite and mesolite, the framework maintains an ordered Al/Si arrangement, but different degrees of Ca-exchange for Na leads to a monoclinic distortion or a tripling of the *b*-axis parameter of the parent orthorhombic natrolite unit cell, respectively. The composition and structural relationship of gonnardite and tetranatrolite remains controversial (Artioli and Galli 1999; Evans et al. 2000; Ross et al. 1992), but they have been reported to have the representative formula $Na_{16-x}Ca_xAl_{16+x}Si_{24-x}O_{80}\cdot nH_2O$ ($0.2 \le x \le 3.9$, $16 \le n \le 25.2$) with disordered Al/Si distributions at the framework T-sites. Paranatrolite is another natrolite analog with a high water content, $Na_{16-x}Ca_xAl_{16+x}Si_{24-x}O_{80}\cdot nH_2O$ or ideally $Na_{16}Al_{16}Si_{24}O_{80}\cdot nH_2O$, $n \sim 24$ (Chao 1980; Ross et al. 1992). It is claimed to transform irreversibly to tetranatrolite upon exposure to the atmosphere after removal from its aqueous environment (Chao 1980). It is therefore believed that tetranatrolite is a dehydration product of paranatrolite (Evans et al. 2000). However, there is no direct structural evidence of a paranatrolite-tetranatrolite transformation nor is there a consensus on an established structural model for paranatrolite (Baur 1991).

We have recently identified two new phases of natrolite with high water contents under hydrostatic pressures (Lee et al. 2001, 2002). This pressure-induced hydration (PIH) of natrolite occurs through the selective sorption of water molecules from the hydrostatic pressure transmitting fluid and increases the zeolitic water contents to 24 and 32 per 80 framework O atoms at 1.0 GPa and above 1.2 GPa, respectively, compared to 16 per 80 framework O atoms at ambient conditions. The structure of the 24 water phase at 1.0 GPa is reminiscent of the proposed structure and phase stability of paranatrolite, although it maintains the Al and Si framework ordering from the parent natrolite framework; we refer to it as an ordered paranatrolite (Lee et al. 2005, this issue). We therefore believe that the hydration-dependent structural changes in tetranatrolite, either with temperature or pressure,

* E-mail: yollee@bnl.gov

may provide a basis to understand its structural relationship to natrolite and paranatrolite. As a first step, we present here a detailed structural evolution of tetranatrolite as a function of temperature-induced dehydration and demonstrate its comparative crystal chemistry to various natrolite phases observed under pressure and temperature.

EXPERIMENTAL METHODS

The tetranatrolite specimen from Mt. Saint-Hilaire was provided by the National Museum of Natural History at the Smithsonian Institution (sample R18930). We use the term tetranatrolite based on the literature for specimens from this locality (Chao 1980; Artioli and Galli 1999; Evans et al. 2000). It is a white polycrystalline overgrowth on the surfaces of natrolite single crystals. Elemental analysis (EPMA) of one of the overgrowth fragments shows an average composition of $Na_{5.85}Ca_{1.90}Al_{9.25}Si_{10.75}O_{40}.xH_2O$. Variable-temperature synchrotron X-ray powder diffraction data for tetranatrolite were obtained from beamline X7A at the National Synchrotron Light Source at Brookhaven National Laboratory. The powdered sample was loaded into a glass capillary of 0.3 mm diameter. The capillary was cut to expose both ends to air to facilitate in situ dehydration and was mounted on the 2nd axis of the diffractometor. A monochromatic beam was selected using a water-cooled channel-cut Ge(111) monochromator. A horseshoe shaped single-crystal heater was placed at the sample position (Brown et al. 1973). The temperature was increased by ca. 10 °C/min to the desired values, and a dwell time of ca. 30 min was used before each measurement. A gas-proportional position-sensitive detector (PSD), gated at the Kr-escape peak, was employed for high-resolution ($\Delta d/d \approx 10^{-3}$) powder diffraction data measurement (Smith 1991). The PSD was stepped in 0.25° intervals between 3° and 50° in 2θ with increasing counting time at higher angles, typically resulting in a 3 hr scan per temperature, and the capillary was spun during the measurement to provide a better powder averaging. The wavelength of 0.7040(1) Å, PSD channel zero, and degree per channel were calibrated using a CeO_2 standard (SRM 674). The resulting variable temperature powder diffraction patterns are shown in Figure 1.

Rietveld structure refinements were performed using the GSAS suite of programs (Toby 2001). The single-crystal structural model by Evans et al. (2000) was used as a starting model for the refinement of the room temperature data. The Na and Ca occupancies at the mixed cation site were fixed based on the elemental analysis results. The Si/Al ratio at the disordered framework tetrahedral sites was also fixed according to the elemental analysis results. The positional refinement of the O atoms for the disordered OW5 molecule at a 16*e* site (0.87, 0.26, 0.18) resulted in unrealistically close distance to the framework O atoms; the OW5 position was later constrained to an 8*d* site (0.87, 0.25, 0.125). Fractional site occupancies of the non-framework O atoms were refined to model the water contents; the occupancy of the fully occupied OW4 site was refined to be slightly higher than 1.0 and hence was fixed to unity. This led to a unit-cell composition of $Na_{5.85}Ca_{1.90}Al_{9.25}Si_{10.75}O_{40}.10.96(5)H_2O$ for the room temperature model. The refined water content is close to that reported for the single-crystal model of Evans et al. (2000). A set of restrained isotropic displacement parameters was refined for the same atomic species. The room temperature structural model was subsequently used as a starting model for the refinement of higher temperature data. Selected refinement results for the room temperature and high temperature structural models are listed in Tables 1 and 2, and the temperature evolutions of the unit-cell lengths and volume are shown in Figures 2 and 3.

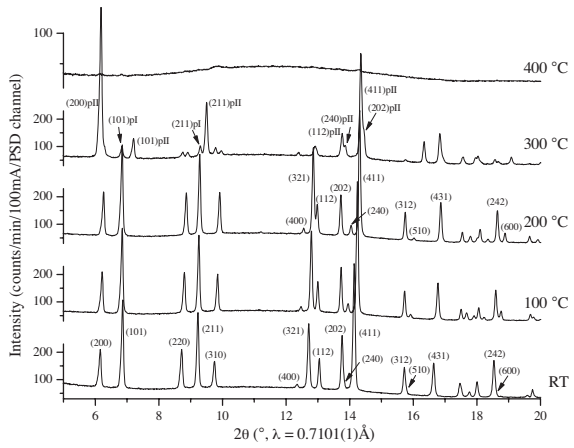

FIGURE 1. Details of the changes in the synchrotron X-ray powder diffraction patterns observed for tetranatrolite as a function of temperature. Two tetragonal phases, partially dehydrated phase I and nearly fully dehydrated phase II, coexist at 300 °C, and the material decomposes above 400 °C.

RESULTS AND DISCUSSION

The room temperature structural model for natural tetranatrolite is characterized by a complete disordering of Si and Al over the framework tetrahedral sites, leading to a tetragonal unit cell with space group $I\bar{4}2d$. The negative charge of the framework is compensated by Na^+ and Ca^{2+} cations occupying the same sites along the channel. In contrast, natrolite shows a complete ordering of Si and Al in the orthorhombic space group *Fdd*2, and only sodium cations occupy a similar site along the channel. Under ambient conditions, tetranatrolite contains more water molecules (close to 22 H_2O per 80 framework O atoms) than natrolite. The disordering of the T-site cations is believed to occur when the Si/Al ratio is less than 1.5 and/or under high-temperature/high water-pressure conditions (Paukov et al. 2002). The fact that natural tetranatrolite from Mt. Saint-Hilaire is observed as an overgrowth on natrolite crystals after dehydration of paranatrolite upon exposure to air suggests that their stabilities are comparable. These phases may transform into each other with minor temperature, pressure, and humidity variations. In fact, three natrolite phases, natrolite (16 H_2O per 80 framework O atoms), ordered paranatrolite (24 H_2O per 80 framework O atoms), and superhydrated natrolite (32 H_2O per 80 framework O atoms) are observed under increasing high water pressures up to 1.5 GPa. The refined water content of tetranatrolite at room temperature and pressure is 21.9(1) H_2O per 80 framework O atoms (Table 1). This is very close to the value expected for naturally occurring paranatrolite and considering the reported volume reduction of ca. 5.5% from paranatrolite to tetranatrolite transformation, a significantly different hydrogen-bonding system is expected in the channels of paranatrolite (Chao 1980). The distribution of water molecules along the channels of tetranatrolite is similar to those of natrolite and superhydrated natrolite. The OW4 site of tetranatrolite is fully occupied, similar to the water site of natrolite at ambient conditions. The partial occupancy of the OW5 site of tetranatrolite accounts for ca. 38% extra water content compared to natrolite. On the other hand, a site similar to OW5 in tetranatrolite is fully filled in the superhydrated natrolite, leading to a doubling of the water content compared to the parent natrolite (Lee et al. 2002).

The temperature-induced dehydration of tetranatrolite at ambient pressure occurs by the selective removal of water molecules from the partially occupied OW5 site. Increasing the temperature up to 200 °C leads to 86% of the OW5 water being lost, whereas the occupancy and distribution of the other water molecules at the OW4 site and the Na/Ca cations remains unchanged (Fig. 3 and Table 1). At 300 °C, the OW5 site becomes empty and the water content becomes the same as that of natrolite at ambient temperature and pressure (16 H_2O per 80 framework O atoms). At this temperature, a new phase (phase II) appears and coexists with the OW5 dehydrated tetranatrolite (phase I). This new phase

TABLE 1. Final refined atomic coordinates for tetranatrolite as a function of temperature

Temperature		Ambient	100 °C	200 °C	300 °C – phase I	300 °C – phase II
space group		$I\bar{4}2d$	$I\bar{4}2d$	$I\bar{4}2d$	$I\bar{4}2d$	$I\bar{4}2d$
$_wR_p$ (%), R_p (%)		2.85, 2.14	2.81, 2.16	3.12, 2.33	3.54, 2.68	
water molecules/u.c.		10.96(5)	9.48(4)	8.41(3)	8.0	1.61(8)
cell length (Å)	*a*	13.1988(1)	13.0666(1)	12.9815(1)	12.9202(10)	13.1503(2)
	c	6.6288(1)	6.6632(1)	6.6808(1)	6.6950(9)	6.2469(1)
T1	*x*	0.0000	0.0000	0.0000	0.000	0.0000
4*a*	*y*	0.0000	0.0000	0.0000	0.000	0.0000
	z	0.0000	0.0000	0.0000	0.000	0.0000
	U_{iso}	0.0080(2)	0.0083(2)	0.0119(2)	0.048(4)	0.0155(4)
T2	*x*	0.0550(1)	0.0560(1)	0.0564(1)	0.051(1)	0.0526(1)
16*e*	*y*	0.1326(1)	0.1336(1)	0.1340(1)	0.136(1)	0.1302(1)
	z	0.6210(1)	0.6220(1)	0.6224(1)	0.625(1)	0.6186(1)
O1	*x*	0.3918(3)	0.3888(3)	0.3842(3)	0.392(2)	0.3949(5)
8*d*	*y*	0.2500	0.2500	0.2500	0.250	0.2500
	z	0.1250	0.1250	0.1250	0.125	0.1250
	U_{iso}	0.0120(5)	0.0155(4)	0.0206(5)	0.026(5)	0.0171(9)
O2	*x*	0.1339(2)	0.1351(2)	0.1356(2)	0.126(1)	0.1378(4)
16*e*	*y*	0.0607(2)	0.0590(2)	0.0591(2)	0.069(1)	0.0433(3)
	z	0.4780(4)	0.4857(3)	0.4881(4)	0.476(2)	0.5635(7)
O3	*x*	0.0526(2)	0.0516(2)	0.0533(2)	0.045(1)	–0.0019(4)
16*e*	*y*	0.0951(2)	0.0943(2)	0.0950(2)	0.097(1)	0.1102(3)
	z	0.8662(3)	0.8664(3)	0.8650(4)	0.862(1)	0.8594(6)
Na	*x*	0.6923(2)	0.6923(1)	0.6925(2)	0.687(2)	–0.0282(5)
8*d*	*y*	0.2500	0.2500	0.2500	0.250	0.250
	z	0.1250	0.1250	0.1250	0.125	0.125
	Occu.	0.731	0.731	0.731	0.731	0.731
	U_{iso}	0.0268(8)	0.0195(6)	0.0240(6)	0.046(8)	0.036(2)
Ca	*x*	0.6923(2)	0.6923(1)	0.6925(2)	0.687(2)	0.026(1)
8*d*	*y*	0.2500	0.2500	0.2500	0.250	0.250
	z	0.1250	0.1250	0.1250	0.125	0.125
	Occu.	0.237	0.237	0.237	0.237	0.237
OW4	*x*	0.1277(4)	0.1287(3)	0.1258(3)	0.134(3)	
8*d*	*y*	0.2500	0.2500	0.2500	0.250	
	z	0.1250	0.1250	0.1250	0.125	
	Occu.	1.0	1.0	1.0	1.0	
	U_{iso}	0.038(1)	0.023(1)	0.027(1)	0.046(8)	
OW5	*x*	0.875(1)	0.895(1)	0.942(6)		0.800(3)
8*d*	*y*	0.250	0.250	0.250		0.250
	z	0.125	0.125	0.125		0.125
	Occu.	0.370(6)	0.185(5)	0.051(4)		0.201(10)
	U_{iso}	0.038(1)	0.023(1)	0.027(1)		0.036(2)

Notes: E.s.d. values are in parentheses. Na and Ca occupancies were fixed according to the elemental analysis results as well as the T-sites to contain 53.7% Si and 46.3% Al. Site occupancy for the OW4 site was fixed to unity; when refined, it becomes slightly larger than unity. Restraints were used to set the isotropic displacement factors, U_{iso} (Å^2), equal for the same atomic species (from ambient temtperature to the 200 °C models) or for the nonframework species (for the 300 °C models). Soft constraints were used for the framework interatomic distances for the 300 °C models (T-O = 1.677 Å and O-O = 2.739 Å). In the 300 °C models, refined phase fractions are 17% and 83% for phase I and phase II, respectively.

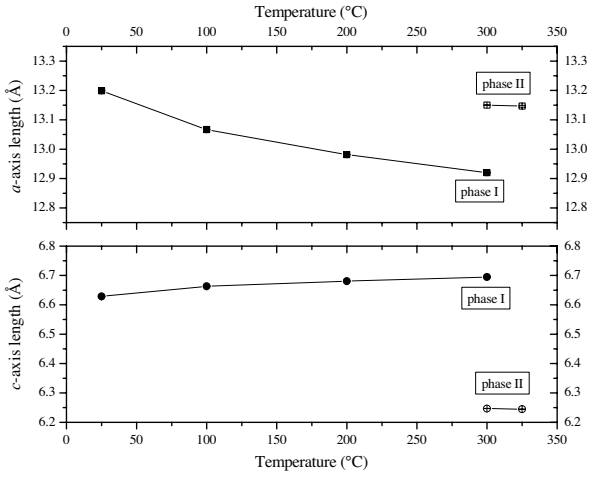

FIGURE 2. Temperature dependence of the unit-cell edge lengths for tetranatrolite. The closed and open symbols represent phase I and phase II, respectively.

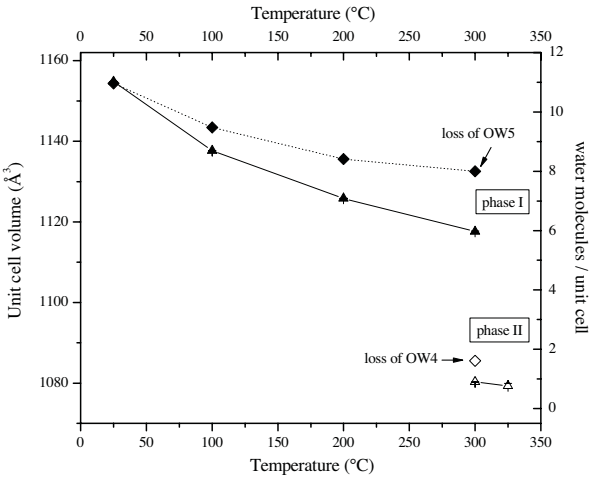

FIGURE 3. Temperature dependence of the unit-cell volume (triangle) and water content (diamond) for tetranatrolite. The closed and open symbols represent phase I and phase II, respectively.

TABLE 2. Selected interatomic distances (Å) and angles (°) for tetranatrolite as a function of temperature

	Ambient	100 °C	200 °C	300 °C – phase I	300 °C – phase II
T1-O3	1.686(3) ×4	1.662(2) ×4	1.677(2) ×4	1.662(6) ×4	1.695(4) ×4
T2-O1	1.702(2)	1.684(2)	1.693(2)	1.655(8)	1.720(4)
T2-O2	1.698(3)	1.686(3)	1.676(3)	1.638(9)	1.637(5)
T2-O2	1.662(3)	1.665(3)	1.670(3)	1.687(13)	1.701(5)
T2-O3	1.699(2)	1.709(2)	1.699(2)	1.666(9)	1.687(4)
Av. T-O*	1.690(1)	1.686(1)	1.685(1)	1.662(5)	1.686(2)
T2-O1-T2	131.2(2)	129.3(2)	125.7(2)	126.7(15)	132.7(4)
T2-O2-T2	136.6(2)	138.2(2)	138.5(2)	140.3(15)	128.2(4)
T1-O3-T2	136.7(2)	138.3(2)	137.9(2)	140.4(7)	126.1(3)
Na-O1	2.613(3) ×2	2.576(2) ×2	2.526(3) ×2	2.61(1) ×2	
Na-O2	2.415(3) ×2	2.415(3) ×2	2.404(3) ×2	2.32(2) ×2	2.450(5) ×2
Na-O3					2.501(4) ×2
Na-OW4	2.436(3) ×2	2.420(3) ×2	2.438(3) ×2	2.39(2) ×2	
Na-OW5	2.41(1)	2.65(2)			2.26(4)
Ca-O2					2.607(6) ×2
Ca-O3					2.504(5) ×2
Ca-OW5					2.97(4)
Na-Ca†					0.72(2)
OW4-O3	2.848(3) ×2	2.851(2) ×2	2.820(3) ×2	2.88(2) ×2	
OW5-O1	2.995(6) ×2	3.11(1) ×2			2.55(1) ×2
OW5-O2	3.161(4) ×2	3.057(4) ×2	2.981(3) ×2		
OW5-O3	2.637(3) ×2	2.598(2) ×2	2.60(2) ×2		
			3.03(4) ×2		
OW4-OW5	2.84(1) ×2	2.98(1) ×2	2.39(8)		
		3.06(2)			

Note: E.s.d. values are in parentheses.
* Standard deviations are computed using

$$\sigma = \frac{1}{n}\left(\sum_{i=1}^{n}\sigma_i^2\right)^{1/2}$$

† Simultaneous occupancy excluded.

shows an abrupt anisotropic framework relaxation with ~1.8% expansion and ~6.7% reduction in the *a*- and *c*-axis parameters, respectively, leading to an overall volume reduction of ~3.3% (Figs. 2 and 3). Concomitant with the anisotropic framework relaxation, the sodium and calcium cations migrate across the channels and order to separate sites (Fig. 4 and Table 1); although the structural model of phase II proposed in Table 1 advocates Na/Ca ordering, it is also possible, based on electron density considerations, to model the two separate Na and Ca sites as mixed Na/Ca (0.73/0.24) cations with site occupancies of 0.63 and 0.37, respectively. This new phase is mostly dehydrated and only a fraction of the former OW4 water is found occupying a site close to the previously empty OW5 site. In natrolite, complete dehydration occurs above 275 °C and results in the formation of metanatrolite, which exhibits similar cation migration and framework collapse (Baur and Joswig 1996). During the selective dehydration of the OW5 water below 300 °C, the disordered Na/Ca cation coordination number decreases from 7 to 6, whereas upon the OW4 dehydration and cation-migration transition, the sodium and calcium coordination number drops to 5 (Table 2).

The disordered aluminosilicate framework responds to the observed temperature-driven chemical changes and rearrangements of the channel contents (Fig. 5). The chain-bridging T-O1-T angle exhibits a gradual decrease during the selective dehydration of the OW5 water and relaxation upon the full loss of water from the OW5 site (Tables 1 and 2). Another useful measure to estimate the degree of the natrolite framework collapse from its ideal geometry is the rotation angle of the fibrous chain, ψ, which is the mean of the angles between the sides of the quadrilateral around the T_5O_{10} (T = Al, Si) tetrahedral building unit projected

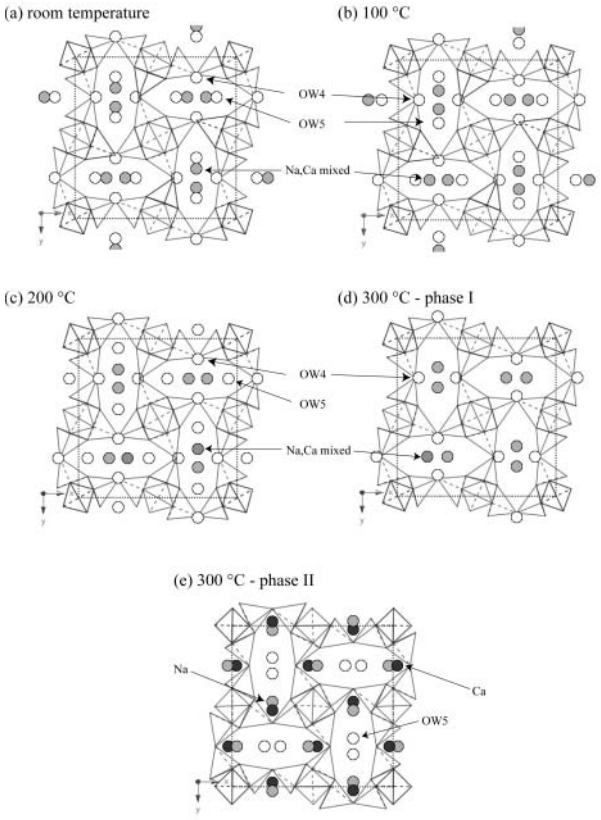

FIGURE 4. Temperature evolution of structural models of tetranatrolite. The empty circles represent water molecules throughout; (**a**-**d**) filled circles are used for the mixed Na/Ca site; (**e**) light and dark circles represent sodium and calcium cations, respectively. The hollow tetrahedra illustrate a disordered distribution of Si/Al atoms at the framework T-sites. The dotted lines define the unit cell.

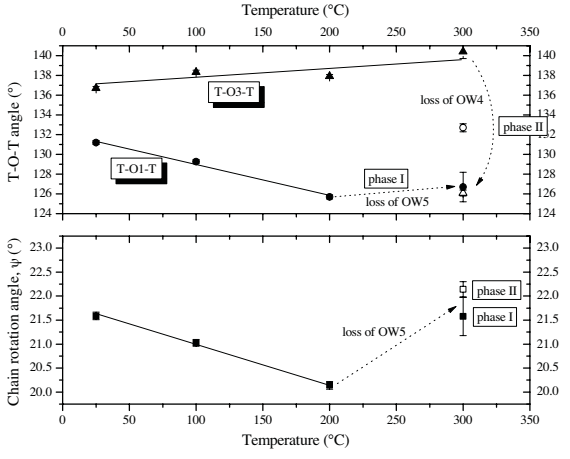

FIGURE 5. Temperature dependence of the T-O-T angles and the chain rotation angle (ψ) for tetranatrolite. The closed and open symbols represent phase I and phase II, respectively.

on the plane perpendicular to the channel (Baur et al. 1990). A larger value of ψ corresponds to a less elliptical channel. The ψ value also shows a gradual decrease followed by a relaxation upon the full loss of the OW5 water (Fig. 5). This demonstrates that the channels become more elliptical during removal of the OW5 water and resume circularity upon its full removal. The ψ angle, however, does not show any noticeable changes upon the OW4 water dehydration and during the cation-migration phase transition. Instead, the T-O3-T angle, which connects the T_5O_{10} tetrahedral building unit along the chain, shows an abrupt decrease with loss of the OW4 water and the cation-migration transition (Fig. 5). We speculate that in the OW4 dehydrated model at 300 °C (phase II), the anisotropic expansion of the *a* parameter compensates for the required changes in the ψ angles on the plane perpendicular to the channels whereas the contraction of the *c* parameter is manifested by the decreasing T-O3-T angle along the chain axis. High-pressure studies of tetranatrolite are underway to investigate a possible overhydration effect and associated structural changes.

ACKNOWLEDGMENTS

This work was supported by an LDRD from BNL (Pressure in Nanopores). Y. Lee thanks the Edward H. Kraus Crystallographic Research Grant from the Mineralogical Society of America. J. Hriljac acknowledges support from the Royal Society. The authors thank J. Post (the Smithsonian Institution) for providing mineral specimens, G. Sheppard (U. Birmingham, U.K.) for EPMA, and A. Langhorn (BNL) for technical support. Research carried out in part at the NSLS at BNL is supported by the U.S. DoE (DE-Ac02-98CH10886 for beamline X7A).

REFERENCES CITED

Artioli, G. and Galli, E. (1999) Gonnardite: Re-examination of holotype material and discredition of tetranatrolite. American Mineralogist, 84, 1445–1450.

Artioli, G., Smith, J.V., and Pluth, J.J. (1986) X-ray structure refinement of mesolite. Acta Crystallographica, C42, 937–942.

Baur, W.H. (1991) Concerning the crystal-structure refinement of paranatrolite published by Pechar, F. Crystal Research and Technology, 26, 169–171.

Baur, W.H. and Joswig, W. (1996) The phases of natrolite occurring during dehydration and rehydration studied by single crystal X-ray diffraction methods between room temperature and 923 K. Neues Jahrbuch für Mineralogie Monatshefte, 4, 171–187.

Baur, W.H., Kassner, D., Kim, C.-H., and Sieber, N.H. (1990) Flexibility and distortion of the framework of natrolite: crystal structures of ion-exchanged natrolites. European Journal of Mineralogy, 2, 761–769.

Breck, D.W. (1984) Zeolite Molecular Sieves. Krieger, Malabar, Florida.

Brown, G.E., Sueno, S., and Prewitt, C.T. (1973) New single-crystal heater for precession camera and 4-circle diffractometer. American Mineralogist, 58, 698–704.

Chao, G.Y. (1980) Paranatrolite, a new zeolite from mont St-Hilaire, Quebec. Canadian Mineralogist, 18, 85–88.

Evans, H.T., Konnert, J.A., and Ross, M. (2000) The crystal structure of tetranatrolite from Mont Saint-Hilaire, Quebec, and its chemical and structural relationship to paranatrolite and gonnardite. American Mineralogist, 85, 1808–1815.

Kvick, A., Stahl, K., and Smith, J.V. (1985) A neutron diffraction study of the bonding of zeolitic water in scolecite at 20K. Zeitschrift für Kristallographie, 171, 141–154.

Lee, Y., Hriljac, J.A., Vogt, T., Parise, J.B., and Artioli, G. (2001) First structural investigation of a super-hydrated zeolite. Journal of the American Chemical Society, 123, 12732–12733.

Lee, Y., Vogt, T., Hriljac, J.A., Parise, J.B., and Artioli, G. (2002) Pressure-induced volume expansion of zeolites in the natrolite family. Journal of the American Chemical Society, 124, 5466–5475.

Lee, Y., Hriljac, J.A., Parise, J.B., and Vogt, T. (2005) Pressure-induced stabilization of ordered paranatrolite: A possible solution to the paranatrolite controversy. American Mineralogist, 252–257.

Meier, W.M. (1960) The crystal structure of natrolite. Zeitschrift für Kristallographie, 113, 430.

Paukov, I.E., Moroz, N.K., Kovalevskaya, Y.A., and Belitsky, I.A. (2002) Low-temperature thermodynamic properties of disordered zeolites of the natrolite group. Physics and Chemistry of Minerals, 29, 300–306.

Pauling, L. (1930) The structure of some sodium and calcium aluminosilicates. Proceedings of the National Academy of Sciences, 16, 453–459.

Ross, M., Flohr, M.J.K., and Ross, D.R. (1992) Crystalline solution series and order-disorder within the natrolite mineral group. American Mineralogist, 77, 685–703.

Smith, G.C. (1991) X-ray imaging with gas proportional detectors. Synchrotron Radiation News, 4, 24–30.

Taylor, W.H., Meek, C.A., and Jackson, W.W. (1933) The structures of the fibrous zeolites. Zeitschrift für Kristallographie, 84, 373.

Toby, B.H. (2001) EXPGUI, a graphical user interface for GSAS. Journal of Applied Crystallography, 34, 210–213.

MANUSCRIPT RECEIVED MAY 4, 2004
MANUSCRIPT ACCEPTED JUNE 28, 2004
MANUSCRIPT HANDLED BY ALESSANDRO GUALTIERI